ACS Sustainable Resource Management

pubs.acs.org/acssrm

Article

Engineered Production of Biochar as Concrete Additives and Its Role in Carbon-Negative Cementitious Composites

Nishad Ahmed, Adhora Tahsin, Warda Ashraf,* Qiangu Yan, and Zhiyong Cai

Cite This: https://doi.org/10.1021/acssusresmgt.5c00158

Read Online

ACCESS | Metrics & More | Article Recommendations | Supporting Information

ABSTRACT: This study explores how biochar with different physicochemical properties affects its performance in cementitious composites and therefore can help to formulate carbon-negative cementitious composites. Eight types of biochar were produced using three methods: (I) air exposure for varying durations, (II) adding K_2SiO_3 during pyrolysis and exposing to air for different durations, and (III) incorporating NaOH at different dosages during pyrolysis. These functionalized biochar samples were added at 30% by weight of the binder, containing slag cement and Ordinary Portland Cement (OPC). Biochar exposed to air for 12 weeks captured more atmospheric CO_2, which accelerated cement hydration and improved compressive strength, achieving 26 MPa after 28 days of sealed curing. The inclusion of K_2SiO_3 or NaOH additives during the pyrolysis process enhanced the performance of biochar as concrete additives. Specifically, K_2SiO_3 improved the performance by achieving a 33 MPa compressive strength, 44% higher than the biochar produced without any additives. The addition of NaOH significantly improved workability and cement hydration by acting as an activator. The addition of 0.5% NaOH to biochar was found to be the optimum dosage, providing a 27% higher compressive strength (29 MPa) compared to the air-exposed biochar batch. The life cycle assessment revealed that all biochar batches had negative carbon footprints, reducing global warming potential by 117%−133% compared to the control (mortar batch without biochar).

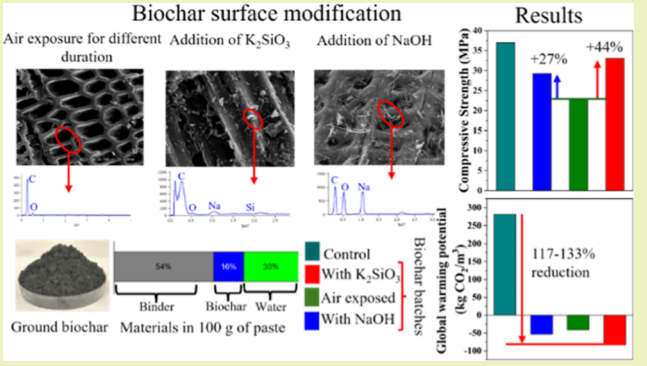

KEYWORDS: *carbon-negative cement, biochar, CO_2 sequestration, modified biochar, life cycle assessment*

Downloaded via 157.51.207.209 on November 29, 2025 at 09:19:34 (UTC).
See https://pubs.acs.org/sharingguidelines for options on how to legitimately share published articles.

INTRODUCTION

Ordinary Portland Cement (OPC) is widely used in various infrastructural applications due to its superior properties, including high strength, cost-effectiveness, and reliability. Globally, its production reaches approximately 4 billion metric tons annually.[1,2] However, its production contributes significantly to CO_2 emissions due to high energy consumption and direct release of CO_2 during manufacturing. Approximately 0.9 to 1.1 tons of CO_2 is released into the atmosphere for every ton of cement production.[3,4] Additionally, the cement industry heavily depends on natural resources.[5] Various stages in the cement lifecycle, such as raw material extraction, processing, and transportation, significantly contribute to greenhouse gas emissions, leading to major environmental concerns.[6] Therefore, there is a crucial need to develop and implement effective strategies for reducing the carbon footprint of the cement and concrete industry. A promising approach to mitigate the growing problem regarding emissions involves the capture and storage of carbon within cement-based materials. In this regard, several studies have shown that biochar can serve as an effective medium for storing carbon in soil.[7,8]

With the global expansion of urban areas and the development of new cities, utilizing biochar as an additive in cementitious materials presents an opportunity to sequester carbon within the civil infrastructure.[9] Biochar is prepared through the thermal decomposition of organic materials in a low-oxygen environment. It is a very stable and carbon-rich material compared to the biomass feedstock it generates from, making it less likely to release carbon back into the atmosphere in the form of CO_2.[10,11] Although the stability of biochar is largely determined by the feedstock characteristics and the conditions of the pyrolysis process, the generation of stable polycyclic aromatic carbon (SPAC) can be effectively achieved through high-temperature pyrolysis.[12] This SPAC remains stable in biochar over a centennial time scale, thereby ensuring carbon sequestration in biochar-based composites for several hundred to thousands of years.[12,13] Such long-term carbon sequestration is not possible to achieve using other wood-based or bio-based composites, as their degradation leads to

Received: March 26, 2025
Revised: October 13, 2025
Accepted: October 16, 2025

© XXXX American Chemical Society

Table 1. Modification of Different Biochar Batches

sample ID	description of sample	air exposure duration	carbon content (%)	BET surface area (m^2/g)	average pore diameter (Å)
GB_1wk	blank biochar	1 week	77.9	290.03	10.27
GB_12wk	blank biochar	12 weeks	77.1	290.03	10.27
K_Si_1wk	promoted with 1 wt % K−2 wt % SiO_2	1 week	87.2	295.65	11.02
K_Si_12wk	promoted with 1 wt % K−2 wt % SiO_2	12 weeks	86.4	295.65	11.02
0.2% Na	promoted with 0.2 wt % NaOH	12 weeks	79.4	275.16	10.53
0.5% Na	promoted with 0.5 wt % NaOH	12 weeks	80.7	273.85	10.95
1% Na	promoted with 1 wt % NaOH	12 weeks	83.6	269.53	11.18
2% Na	promoted with 2 wt % NaOH	12 weeks	86.3	263.32	11.22

the release of carbon as carbon dioxide or methane into the atmosphere.[14] Depending on the production process and feedstock type, biochar can reduce net greenhouse gas emissions by around 870 kg CO_2 eq per ton of dry feedstock, primarily through the carbon capture and storage capabilities of biomass.[15] Due to this high carbon sequestration capacity, researchers are now focusing on using biochar in cementitious materials to achieve carbon neutrality.

Several studies have explored the impact of biochar on the mechanical and microstructural properties of cementitious composites. Adding a small dosage of biochar (0.5%−2.5%) can enhance the mechanical properties of mortar samples,[16−18] which is insufficient to achieve carbon neutrality. As a result, it is also important to assess the effects of a high biochar content (more than 10%) on the properties of cement-based materials. However, adding a high dosage of biochar drastically reduces the mechanical performance of composites due to its high porosity and water retention capacity.[19,20] To address these challenges, modification of biochar properties emerges as a crucial strategy to enhance its compatibility with cementitious materials.[21] The majority of studies utilized ground biochar as a filler material or used different pyrolysis temperatures to modify the surface properties of biochar. For example, Tan et al. investigated the effect of pyrolysis temperatures ranging from 400 °C to 700 °C on the mechanical and microstructural properties of cementitious composites, incorporating up to 10% biochar as a replacement for OPC.[22] Similarly, Chen et al. also examined the properties of composites after adding biochar in the cementitious composites (up to 5% by wt. of binder), which was pyrolyzed at different temperatures (300 °C to 550 °C).[23] However, Gupta et al. used biochar-coated polypropylene fibers to investigate the strength and permeability of mortar samples.[24] In these studies, biochar was mainly used in the cementitious composites in three different ways: (i) replacement of OPC, (ii) replacement of fine aggregate, or (iii) addition of biochar (with respect to the weight of binder) in the cementitious composites. However, beyond adjusting pyrolysis conditions, recently, researchers have explored other modification strategies to enhance the adsorption capacity and surface characteristics of biochar, such as alkaline treatment, steam treatment, physical activation, and acidification of biomass feedstocks.[25−28] For example, Chen et al. investigated the influence of seven alkaline additives on the biomass pyrolysis, revealing significant enhancements in char formation and surface functionality.[29] In addition to chemical pretreatment, several studies have examined the aging behavior of biochar under different atmospheric conditions. These revealed that biochar's surface chemistry and functional groups evolve with long-term air exposure, which can influence its performance.[30,31] Most recently, Yan et al. investigated the combined effect of pyrolysis temperature and alkaline pretreatment of biochar with NaOH to enhance its effectiveness in sustainable and efficient lead remediation.[32] However, to date, the combined effects of alkaline pretreatment and extended aging of biochar on the performance of carbon-negative cementitious composites remain unexplored.

The primary objective of this research work is to investigate the impact of incorporating eight different types of engineered biochar on the workability, hydration kinetics, and mechanical and microstructural properties of carbon-negative cementitious composites. For this, the biochar batches were divided into three categories to evaluate: (I) the effect of air exposure duration on biochar properties, (II) the combined effect of K_2SiO_3 dosages under varying air exposure durations, and (III) the influence of NaOH dosage on biochar properties. Overall, this paper describes the endeavor to develop a multifunctional additive for producing carbon-negative cementitious composites using biochar.

MATERIALS AND METHODS

Raw Materials. In this study, slag cement, OPC, river sand, and biochar were used as raw materials. The chemical composition of slag cement and OPC was determined through X-ray fluorescence (XRF) analysis (Table S1). A blended binder was produced by mixing slag cement and OPC in a 1:1 ratio.

Biochar Production and Processing. Pine particles were used as feedstock in this work. The proximate and elemental analyses of the pine particle feedstock are listed in Table S2. Alkaline pretreatment of the pinewood feedstock was accomplished via dry impregnation, which was followed by a previously published work.[32] This process involved mixing potassium silicate (K_2SiO_3) or sodium hydroxide (NaOH) solutions of varying concentrations with pine particles. The liquid-to-solid mass ratio of 2.44:1 was optimized based on preliminary tests. The mixture was stirred continuously for 30 min. Following this initial mixing period, the feedstock was stirred gently at regular intervals over the next 2 h, rather than being mixed continuously. This periodic stirring was carried out to promote uniform mixing and ensure that the alkaline solution was evenly distributed throughout the feedstock before pyrolysis. To facilitate deeper penetration of the K_2SiO_3 and NaOH solution into the pine particles, a vacuum process was employed for 10 min. The mixture was then stored in a dark condition for 24 h, starting from the initial mixing. Subsequent air drying for 24 h, followed by oven drying at 105 °C for another 24 h, resulted in the preparation of materials with 1 wt % K−2 wt % SiO_2 (K to Si ratio 1:2) and NaOH dosage of 0.2, 0.5, 1.0, and 2.0 wt % of pine particles. The dried pine particle samples were pyrolyzed in a muffle furnace at 450 °C with a heating rate of 20 °C/min under a nitrogen flow (0.2 SLPM) for 1 h. The obtained biochar samples were labeled and are listed in Table 1. According to Table 1, biochar samples were kept in the air for 1 or 12 weeks in a typical laboratory environment with a temperature of around 70 °F and a humidity of around 60%. These selected time intervals of 1 and 12 weeks enable us to observe both the short-term and long-term stages of biochar aging under typical atmospheric conditions. For example, a previous study found that sludge-derived biochar aged in air for 30−120 days at different temperatures

https://doi.org/10.1021/acssusresmgt.5c00158
ACS Sustainable Resour. Manage. XXXX, XXX, XXX−XXX

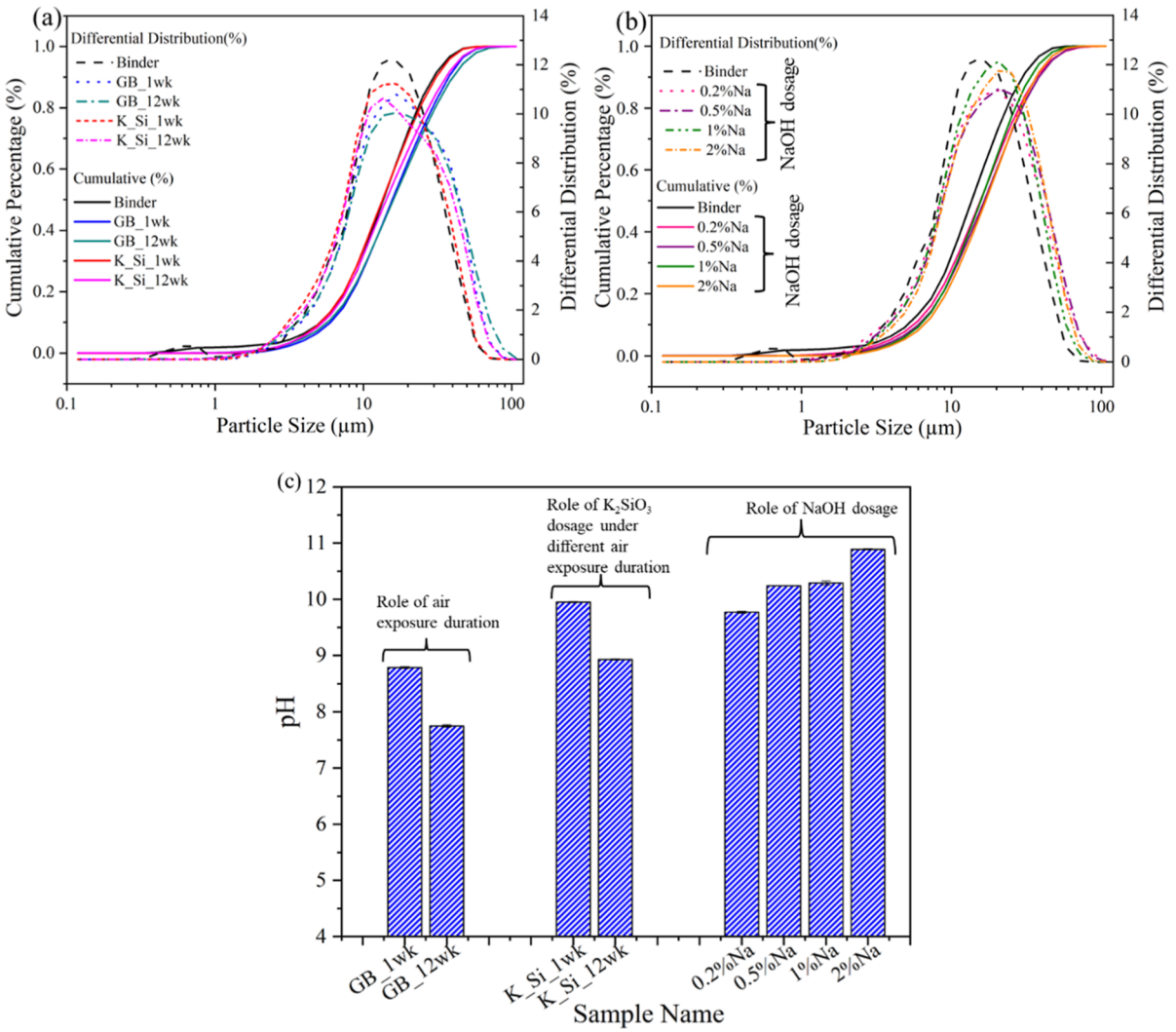

Figure 1. (a,b) Particle size distribution. (c) pH measurement of different biochar batches.

exhibited a higher cation exchange capacity (CEC), which was attributed to the enriched surface density of carboxyl groups.[33] Generally, fresh biochar has fewer oxygen-containing functional groups, such as hydroxyl (−OH), carboxyl (−COOH), and carbonyl (−C═O) on its surface, and it is more hydrophobic. However, when the fresh biochar is aged in air, oxygen and moisture will penetrate its porous structure and react with the surface carbon atoms to generate oxygen-containing functional groups.[30] The aged biochar is more polar and hydrophilic due to the oxygen-containing functional groups. This can significantly alter its interactions with water and metal ions.[31,34] Carboxyl and hydroxyl groups are acidic and can deprotonate, creating negatively charged sites on the biochar surface. This increases the cation exchange capacity (CEC), improving the biochar's ability to retain positively charged mineral ions (like Ca^{2+}, Al^{3+}, Mg^{2+}, K^{+}).[35] However, Table 1 also represents the carbon content, BET surface area, and average pore diameter of different biochar samples after pyrolysis. As shown in Table S2, the, the pine feedstock contains approximately 51.3% elemental carbon. When treated with K_2SiO_3 or NaOH and then pyrolyzed, the carbon content of biochar increased up to 12% (Table 1) compared to the untreated biochar (GB_1wk and GB_12wk). These treatments may increase char formation and reduce the formation of volatile organic compounds during pyrolysis, resulting in a higher retention of fixed carbon.[36] Furthermore, the alkali additives may reduce the decomposition of carbonaceous material into gases and tar, increase the catalytic effect of pyrolysis, thereby increasing biochar yield and its fixed-carbon content.[37] This enhanced carbon retention is necessary because it directly improves the biochar's capacity to sequester carbon in the cementitious matrix and lowers the global warming potential (GWP) of the composites. It is important to note that the alkalis were incorporated into the biomass feedstock prior to pyrolysis at dosages of 0.2−2 wt % NaOH and 1 wt % K−2 wt % SiO_2 relative to the feedstock mass. During pyrolysis, substantial mass loss occurs due to the release of volatile compounds. As a result, the actual amount of alkali retained in the produced biochar differs from the initial amount of alkali added in the feedstock, and the effective alkali content in the biochar-modified batches cannot be considered equivalent to the amount added on a feedstock basis. Determining the precise residual alkali content after pyrolysis would require a detailed chemical characterization, which was beyond the scope of this study. We therefore recognize this as a limitation of the present work and a valuable direction for future research. For clarity, the dosages and sample names reported in Table 1 are based on the amounts of alkalis added to the feedstock before pyrolysis.

Sample Preparation. In this experiment, eight different types of biochars were used to prepare carbon-negative composites. The biochar particles were finely ground for 1 h using a ball mill with a rotational speed of 2520 rpm. The particle size distribution of the blended binder and different ground biochar batches is given in Figure 1a,b, and the d_{50} value is provided in Table S3. Our primary objective was to produce carbon-negative cementitious composites using different types of modified biochar; therefore, we aimed to minimize the content of the OPC due to its high global warming potential (GWP) value while ensuring that the mechanical properties

https://doi.org/10.1021/acssusresmgt.5c00158
ACS Sustainable Resour. Manage. XXXX, XXX, XXX−XXX

remained acceptable. By blending slag cement and OPC in a 1:1 ratio based on our previous study,[21] we achieved a significant reduction in GWP without compromising the overall strength of the composites. 30% biochar (by weight of binder) was added to this blended binder to obtain the carbon-negative batch. As presented in Table S4, the addition of biochar resulted in a reduction in both the binder (OPC + Slag) and the fine aggregate content needed to produce 1 m^3 mortar. But the sand-to-binder ratio and the water-to-binder ratio of the mortar mixes were kept constant. Thus, biochar acts as a partial binder replacement, as well as a partial replacement for the fine aggregate in the mixture. The ratio of the fine aggregate-to-binder was 2.75, and the water-to-binder ratio was 0.55. The detailed mix design and mixing procedure for mortar and paste samples are described in Table S4 and Section 1, respectively. All samples were removed from their molds 24 h after casting and kept in sealed curing condition using plastic wrap for 7 and 28 days.

Test Procedures. The workability of different mortar batches was evaluated using a flow table test as per ASTM C1437.[38] The workability value was recorded immediately after the mixing process.

The compressive strengths of 50 mm cube mortar samples were measured as per ASTM C109[39] after 7 and 28 days of sealed curing.

An isothermal calorimeter test was carried out to investigate the hydration kinetics of the paste samples. Around 5 g of dry mixtures (slag, OPC, and biochar) from each batch were placed into the glass ampoules, which were then inserted into the calorimeter chamber (TAM AIR, TA Instruments). The heat flow signals of each chamber were stabilized after 45 min and then water was injected into the mixture using syringes, and the heat of the reaction began recording instantly afterward. The test was carried out at 25 °C for 7 days.

The commercially available TGA 550 TA Instruments was used to perform thermogravimetric analysis (TGA) of the raw biochar and the 28 days of sealed cured paste samples in this study. This instrument was calibrated for a sample size of 10 mg to 100 mg. To obtain repeatable data, approximately 30 to 40 mg of the sample was used for this study. A finely pulverized sample was put into a platinum pan and subjected to an isothermal condition for 3 min at 25 °C. After that, the temperature was increased to 980 °C at a rate of 15 °C per minute. N_2 was used throughout the process to confirm an inert environment.

The Fourier transform infrared (FTIR) spectra of raw biochar and 28 day sealed cured paste samples were collected using a Nicolet iS5 FTIR instrument fitted with an attenuated total reflectance (ATR) accessory. The spectra were recorded over a frequency range of 400−4000 cm^{-1} with a resolution of 4 cm^{-1} and 32 scans per sample.

Scanning electron microscopy (SEM) and energy dispersive spectroscopy (EDS) analysis of various unground biochar samples and 28 days sealed cured paste samples was done to observe the interaction between the biochar particles and the addition of Na, K, and Si (Table 1) using the HITACHI 3000 N SEM. Before taking the SEM images, the samples were coated with Gold (Au)−platinum (Pt). The instrument was operated in a high vacuum mode with an accelerated voltage of 25 kV and a working distance of around 10−15 mm. The same working distance was used to collect the EDS data point.

Global Warming Potential (GWP). SimaPro software was utilized to calculate the GWP of mortar mixes with various engineered biochar, and the analysis was conducted using the TRACI (The Tool for the Reduction and Assessment of Chemical and Other Environmental Impacts) method. The emission data for all raw ingredients, except biochar, including OPC, slag, sand, water, NaOH, KOH, and SiO_2, were obtained from the Ecoinvent 3 database (Section 2 and Table S5). The carbon content in various engineered biochar samples was analyzed, ranging from 77% to 87%, as shown in Table 1. The equivalent CO_2 captured in their structure was calculated based on eq 1, which resulted in a carbon sequestration capacity of different biochar-containing batches from −3.20 to −2.83 kg CO_2 equiv/kg of biochar. However, to calculate the net GWP value of biochar samples, the biochar production emission should also be considered. There are two main steps involved in producing biochar: pretreatment of the feedstock and preparation of the biochar. Feedstock pretreatment typically involves processes such as drying, storage, grinding, chipping, or pelletizing,[40] whereas the carbon footprint of biochar production is mainly determined by the energy sources used to operate the pyrolysis process. For example, Puettmann et al.[41] used three different types of portable systems, such as the Oregon kiln, biochar solutions incorporated (BSI), and an air-curtain burner. In the BSI system, different energy sources were applied depending on the location, including grid electricity for urban settings and diesel- or gasifier-based generators for near-forest sites,[41,42] while another study utilized natural gas to pyrolyze wood sawdust.[9] Depending on the energy system employed, such as a gasifier- or diesel-powered generator, CO_2 emissions associated with biochar production were estimated to range from 0.2 to 0.8 kg CO_2 equiv/kg of biochar.[41] In this study, we considered the production emission of biochar to be 0.7 kg CO_2 equiv/kg of biochar.[43] The net GWP values of different biochar batches were calculated based on eq 2 after considering carbon sequestration capacity, production emission of different biochar samples, and the addition of NaOH/KOH + SiO_2 in the biochar samples in the samples, which resulted in a net GWP ranging from −2.39 to −2.13 kg CO_2 equiv/kg (Section 2 and Table S6). The CO_2 captured by the binder matrix was also assessed by using TGA and deducted from the total CO_2 emissions of the mortar mixes. Equation 3 is used to calculate the total mortar GWP in kg of CO_2 equiv/m^3 of mortar for the control and all biochar-containing batches. In this equation, first, the CO_2 emission from raw materials, except biochar, was calculated by multiplying the values from Tables S4 and S5. Second, multiplying Table S4 (kg/m^3 of mortar) by Table S6 (kg CO_2 equiv/kg) provided the CO_2 sequestration of different biochar samples in mortar (kg CO_2 equiv/m^3 of mortar), and third, CO_2 sequestration in mortar (kg CO_2 equiv/m^3 of mortar) is obtained from the TGA—Figure 7. Table S7 represents the total mortar GWP values of different batches in kg CO_2 equiv/m^3 of mortar, obtained from eq 3.

$$\text{Carbon sequestration of biochar (kg}CO_2\text{ equiv/kg of biochar)} = \frac{44}{12} \times \text{carbon content (\%) in biochar} \quad (1)$$

$$\text{Net GWP (kg}CO_2\text{ equiv/kg of biochar)} = \text{carbon sequestration of biochar + production emission of biochar + emission from the addition of NaOH/KOH + } SiO_2 \quad (2)$$

$$\text{Total mortar GWP (kg}CO_2\text{ equiv/m}^3\text{)} = CO_2\text{emission from raw material (binder + fine aggregate + water) production + } CO_2\text{ sequestration by biochar + } CO_2\text{ sequestration in binder (calculated from TGA-Figure7)} \quad (3)$$

RESULTS AND DISCUSSION

Raw Biochar Characterization. The pH measurements of different biochar batches, as illustrated in Figure 1c, indicate that both GB_12wk and K_Si_12wk batches exhibited pH values lower than those of their respective 1 week batch. This reduction in pH is attributed to prolonged exposure to air, which facilitates increased CO_2 adsorption by biochar.[9,44] The dissolved CO_2 reacts with water to form carbonic acid (H_2CO_3), which decreases the pH. In contrast, the pH values of the Na-containing biochar batches increased as the Na dosage increased, demonstrating its alkalinizing effect.

This observed difference can be attributed to the adsorption of atmospheric CO_2 by the biochar over time. Biochar, due to its high surface area and porosity, is capable of capturing CO_2

https://doi.org/10.1021/acssusresmgt.5c00158
ACS Sustainable Resour. Manage. XXXX, XXX, XXX−XXX

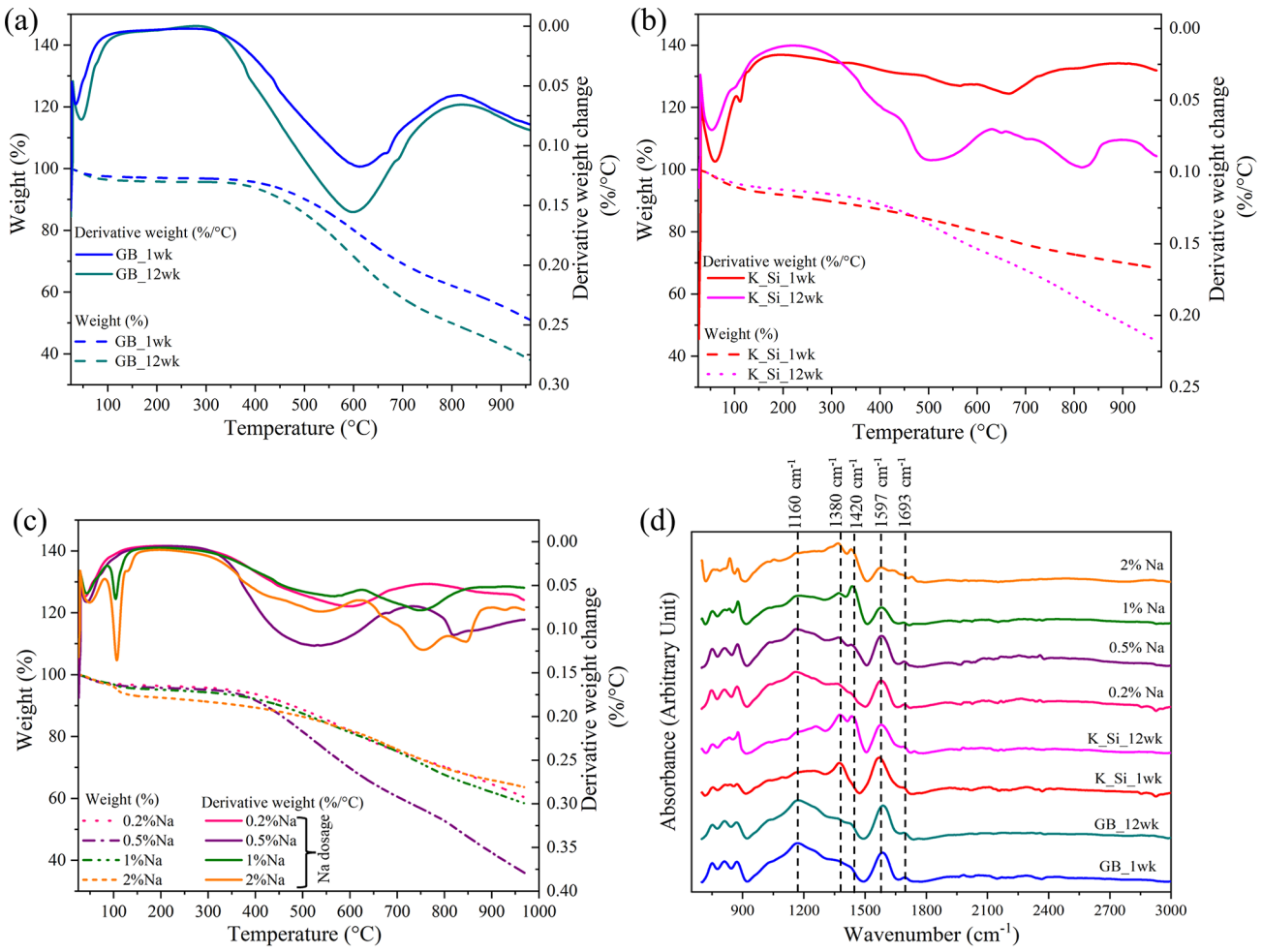

Figure 2. Thermogravimetric analysis of different raw (unground) biochar batches: (a) effect of biochar exposure to air for different durations, (b) effect of K_2SiO_3 dosage in biochar under varying air exposure durations, (c) effect of NaOH dosage in biochar, and (d) FTIR spectra of raw (unground) biochar.

from the surrounding environment.[9] Since CO_2 is captured primarily by adsorption onto the pore structure, there is no significant alteration of the biochar's morphology or its physical and chemical properties, even when its pores become saturated with CO_2.[45,46] This is further supported by the FTIR results (Figure 2d) and SEM/EDS analysis (Figure 3a), which showed no significant differences between the GB_1wk and GB_12wk batches. The GB_12wk batch, which was exposed to air for 12 weeks, experienced a longer duration for CO_2 adsorption, resulting in a higher accumulation of CO_2 within its pores. As shown in Figure 2a, the weight loss after approximately 300 °C in the GB_1wk batch can be attributed mainly to the thermal decomposition of biomass,[32] assuming no substantial CO_2 adsorption within this time period. However, greater weight loss was observed in the GB_12wk batch. Considering that both these batches are expected to have the same biomass content, the increased weight loss in the GB_12wk batch is attributed to the release of adsorbed CO_2.[9]

Mass losses in the range of 550 °C to 900 °C can be attributed to the decomposition of the carbonate in the sample.[21,47] The biochar decomposition also starts from around 300 °C.[32] Therefore, in Figure 2b,c, mass losses after 700 °C range are especially linked to the decomposition of K_2CO_3 and Na_2CO_3 as well as biomass itself.[47,48] In Figure 2b, the K_Si_12wk batch also exhibited higher weight loss after 550 °C than the K_Si_1wk batch, confirming that extended exposure to atmospheric air promotes further carbonate formation. The additional formation of K_2CO_3 in the K_Si_12wk batch was further validated through FTIR analysis (Figure 2d), which revealed an additional peak around 1420 cm^{-1} after 12 weeks of air exposure—corresponding to the stretching vibration of the carbonate ion (CO_3^{2-}).

Figure 2c represents the thermal analysis plot of biochar with varying NaOH dosages. The mass loss after 600 °C was notably higher for the 2% Na batch than for the other batches. The 2% Na batch, due to its higher NaOH content, likely converted to Na_2CO_3 while being exposed to air for 12 weeks. Therefore, the increased weight loss can be attributed to the decomposition of Na_2CO_3. This observation is also supported by FTIR and SEM/EDS analysis later in this section, which further confirms the formation of carbonate compounds in the Na-containing biochar.

The FTIR spectra of the raw biochar are shown in Figure 2d. The absorbance bands observed in GB_1wk and GB_12wk, located around 1160−1170 cm^{-1}, correspond to the stretching vibrations of the C−O−C bond in undecomposed cellulose.[49] Additionally, the band at around 1600 cm^{-1} is associated with carbon−carbon (C═C) bonds linked to carboxylic groups, and the peak at 1693 cm^{-1} is associated with the stretching of

https://doi.org/10.1021/acssusresmgt.5c00158
ACS Sustainable Resour. Manage. XXXX, XXX, XXX−XXX

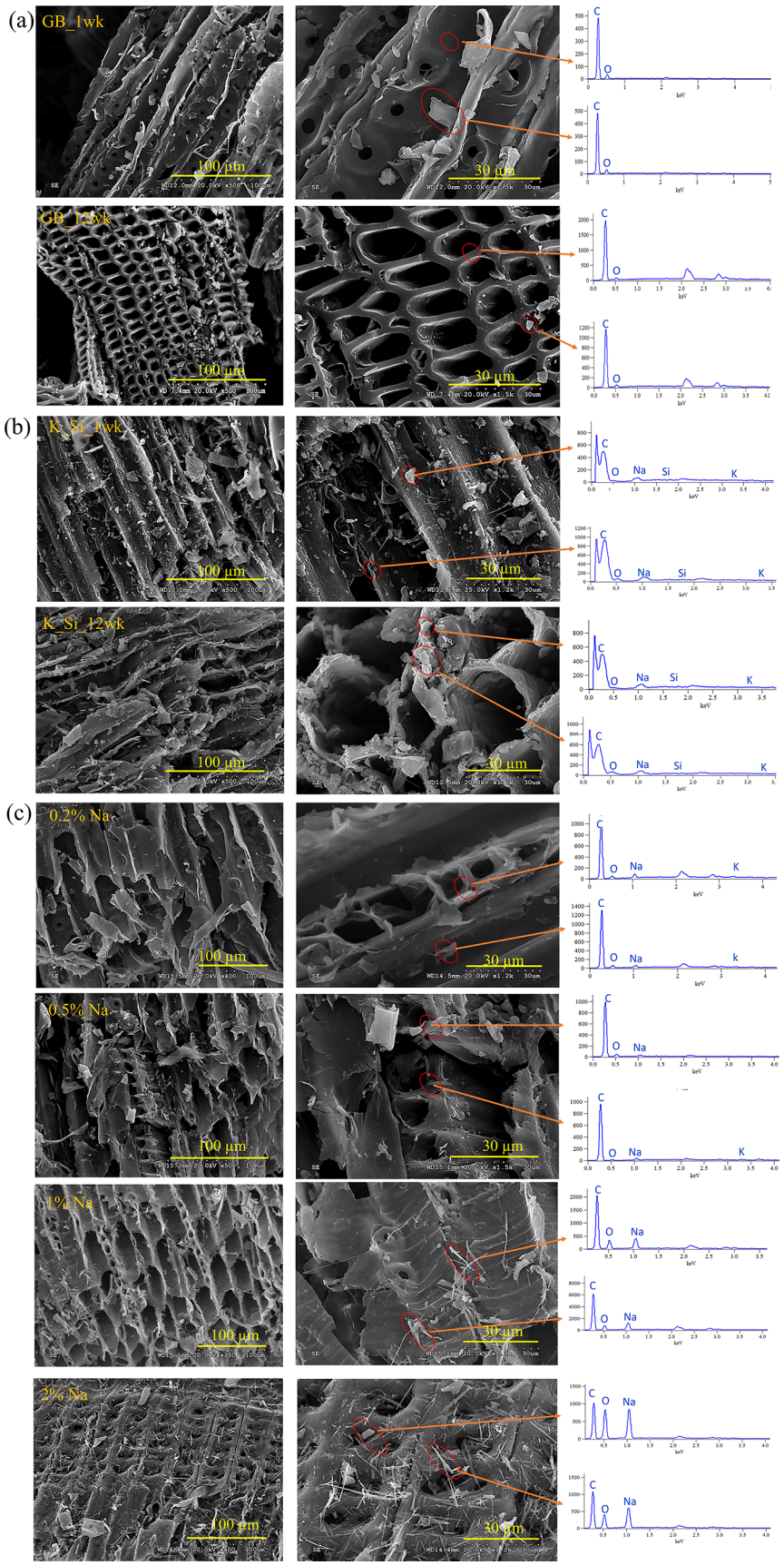

Figure 3. High- and low-resolution SEM images and EDS analysis of different raw (unground) biochar batches: (a) effect of biochar exposure to air for different durations, (b) effect of K_2SiO_3 dosage in biochar under varying air exposure durations, and (c) effect of NaOH dosage in biochar.

https://doi.org/10.1021/acssusresmgt.5c00158
ACS Sustainable Resour. Manage. XXXX, XXX, XXX−XXX

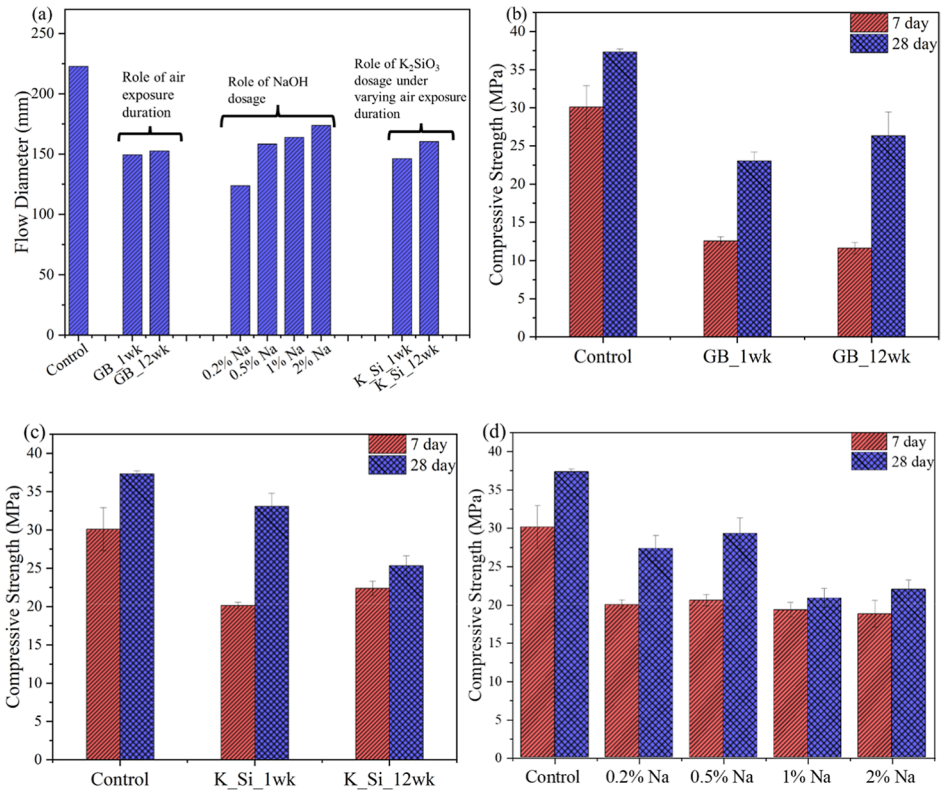

Figure 4. (a) Flow diameter and (b–d) compressive strength of different batches: (b) effect of biochar exposure to air for different durations, (c) effect of K_2SiO_3 dosage in biochar under varying air exposure durations, and (d) effect of NaOH dosage in biochar.

carbonyl bonds of the conjugated ketone or carboxylic group.[50] However, the addition of K_2SiO_3 in K_Si_1wk biochar led to the formation of an additional band around 1380 cm^{-1}, corresponding to the asymmetric stretching of carbonate ions ($-CO_3^{2-}$).[51] After 12 weeks of exposure to air, the K_Si_12wk biochar exhibited a new peak at 1420 cm^{-1} due to the stretching vibration of CO_3^{2-}, indicating increased carbonation of the alkali ion (K^+) over time.[52] Similar observations were noted in the Na-containing biochar, where the absorbance band at 1160 cm^{-1} was gradually overshadowed by the CO_3^{2-} vibration at 1380 cm^{-1} and 1420 cm^{-1} with increasing NaOH dosage, which was most pronounced in the 2% Na biochar. These FTIR results helped to differentiate two distinct CO_2 uptake mechanisms by the biochar batches. For the ground biochar (GB) batches, the absence of new carbonate bands or notable changes in functional groups indicates that the CO_2 uptake (observed in TGA analysis) was primarily physical. In contrast, for the alkali-treated batches, FTIR and TGA results together substantiated the formation of carbonate due to chemical reactions with atmospheric CO_2.

Figure 3a represents the SEM/EDS analysis of GB_1wk and GB_12wk batches. No significant changes were observed in the morphology of biochar particles after keeping them in air for 12 weeks. The morphology of the biochar surface after adding K_2SiO_3 in biochar is shown in Figure 3b. As per the EDS point analysis, SiO_2 agglomeration on the biochar surface was comparatively higher in the K_Si_12wk batch than in the 1 week batch containing the same K–Si addition. The SEM images, along with EDS point analysis of biochar batches with varying Na dosages, are shown in Figure 3c. The SEM and EDS analyses revealed no significant change in the morphology of the biochar surface after adding 0.2% and 0.5% NaOH dosages. However, with the higher NaOH dosages (1% and 2%), needle-shaped structures were observed on the biochar surface, indicating Na-based compound formations, which were adsorbed onto the biochar surface.

Effects of Biochar Modification on Workability. Figure 4 represents the workability measurements for the different biochar batches. The control batch, prepared without biochar, exhibited the highest flow value of 222.75 mm, which drastically reduced after the incorporation of biochar. Among the biochar batches, the 2% Na batch recorded the highest workability, achieving 78% of the control batch, while the 0.2% Na batch exhibited the lowest workability. Furthermore, the K_Si_1wk and K_Si_12wk batches also exhibited significant reductions in workability of 33% and 29%, respectively, compared to the control. As shown in Figure 4a, negligible differences were observed between the GB_1wk and GB_12wk batches, which yielded workability values of 149.25 and 152.5 mm, respectively. This significant drop in workability is caused by biochar's porous structure and angular particle shape, which increased water retention capacity and hindered cement particle flow by reducing free water.[11] During mortar preparation, biochar absorbed a portion of the mixing water by hydrogen bond, which reduced the workability of the mortar mix.[22] However, the workability increased gradually as the NaOH dosage in biochar was increased. The 2% Na batch showed a workability 40% higher than that of the 0.2% Na batch. Na, added with biochar, formed NaOH in the fresh mortar mix, which worked as an activator for the slag. Increasing the NaOH dosage enhanced slag dissolution, producing negatively charged aluminate and silicate ions that repel each other, thereby improving the initial workability of the mortar mix.[53]

https://doi.org/10.1021/acssusresmgt.5c00158
ACS Sustainable Resour. Manage. XXXX, XXX, XXX–XXX

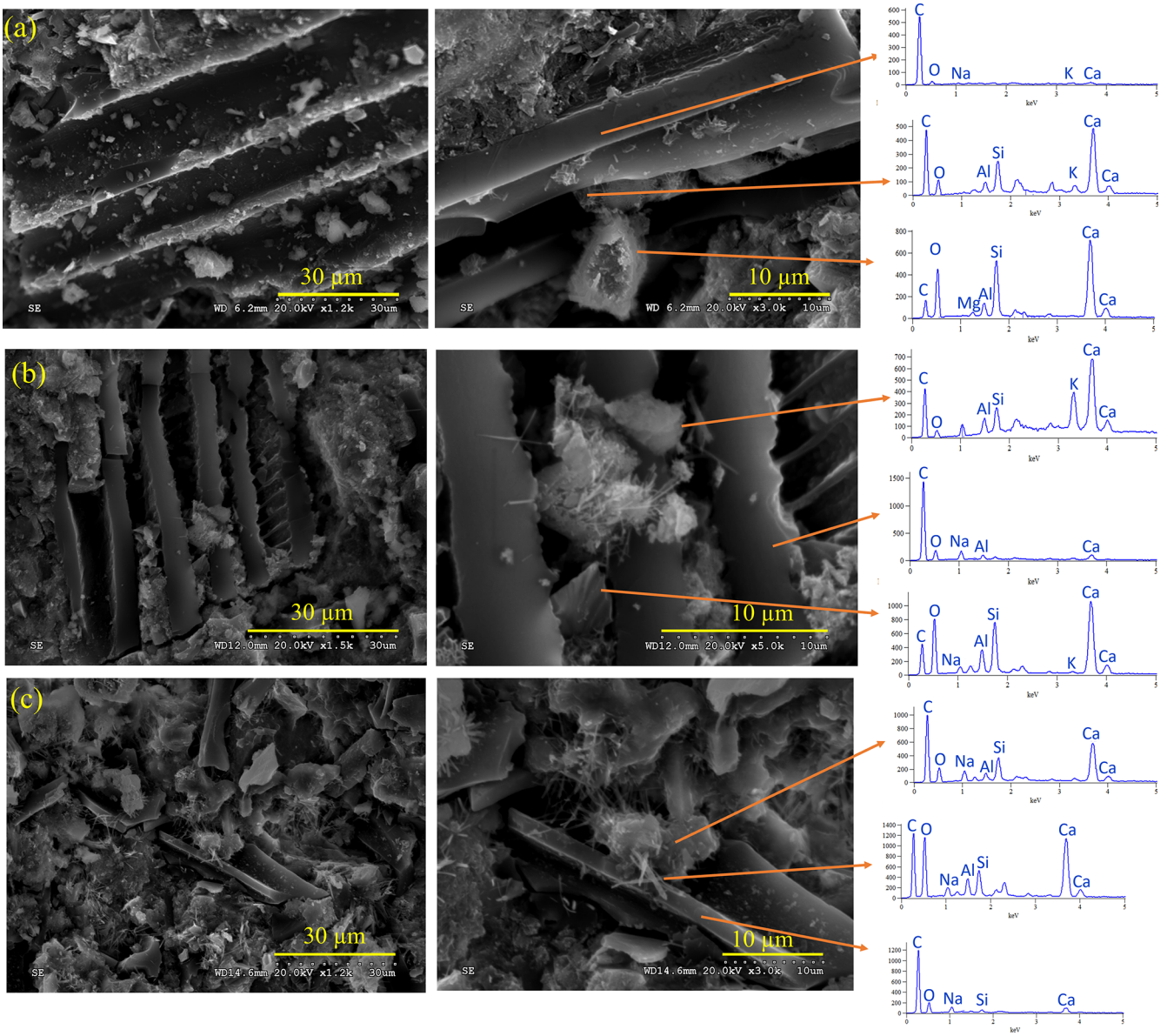

Figure 5. High- and low-resolution SEM images and EDS analysis of 28 day sealed cured different paste samples: (a) GB_12wk, (b) K_Si_12wk, and (C) 2% Na batches.

Effects of Modified Biochar on the Compressive Strength of Cementitious Composites. Figure 4b represents the effect of biochar exposure duration to air on the compressive strength of the 7 and 28 day sealed cured mortar samples. The 28 day compressive strength of GB_1wk and GB_12wk biochar batches was 62% and 70% of the control batch, respectively. This reduction can be attributed to the dilution effect as 30% of biochar was added to the mortar mix. As a result, the overall amount of available binder decreased for hydration.[21] The SEM/ EDS analysis (Figure 5) revealed the formation of cement hydration products on the biochar surface, indicating that biochar could serve as an additional nucleation site for cement hydration.

Figure 4c compares the compressive strength of the K_Si_1wk and K_Si_12wk biochar batches with the control batch. The K_Si_1wk batch exhibited the highest compressive strength among all the biochar-containing batches. Specifically, its compressive strength was 44% higher than that of the GB_1wk batch and reached 89% of the control batch's strength after 28 days. The superior strength of the K−Si-containing biochar batch was attributed to the pozzolanic properties of the added silica, which reacted with calcium hydroxide to produce calcium silicate hydrate (C−S−H),[54] in addition to the alkali activation effect of K due to the relatively high pH of this biochar batch as observed in Figure 1. This contributed to the improved compressive strength at later stages. For example, the 28 day compressive strength of the K_Si_1wk batch increased by 65% compared with the 7 day strength. However, the strength of the K_Si_12wk biochar batch did not increase significantly after 28 days. This is due to the higher agglomeration of SiO_2 on the biochar surface due to the long-term exposure to the air, which was observed from the SEM image of this batch (Figure 5b) and conversion of KOH to K_2CO_3 due to the atmospheric carbonation as apparent by the reduced pH of this biochar batch in Figure 1.

Figure 4d demonstrates the effect of varying the NaOH dosage in biochar on the compressive strength of mortar batches. The incorporation of 0.2% Na and 0.5% Na in biochar

https://doi.org/10.1021/acssusresmgt.5c00158
ACS Sustainable Resour. Manage. XXXX, XXX, XXX−XXX

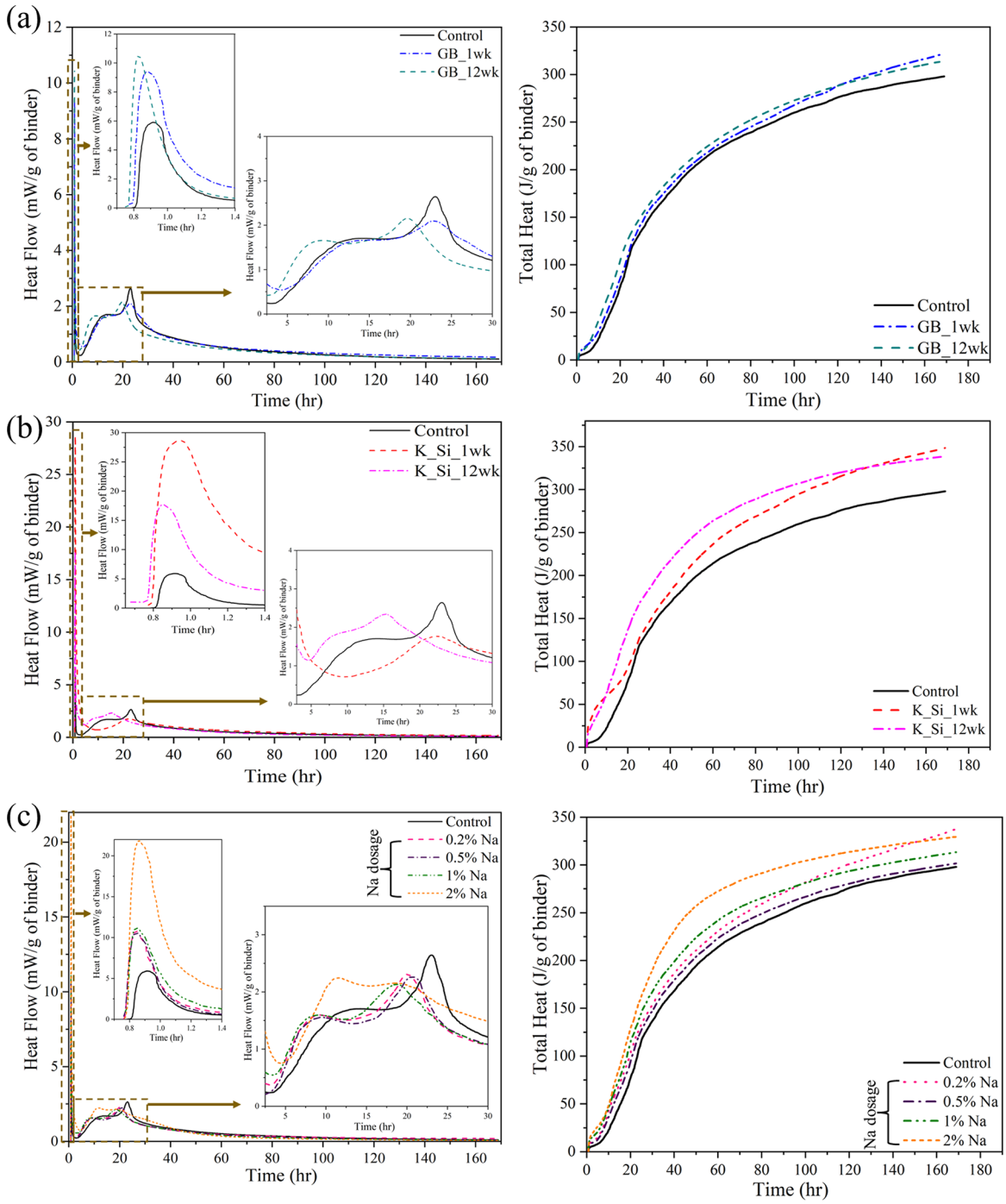

Figure 6. Total heat release and heat flow for the paste samples containing different modified biochar batches: (a) effect of biochar exposure to air for different durations, (b) effect of K_2SiO_3 dosage in biochar under varying air exposure durations, and (c) effect of NaOH dosage in biochar.

enhanced compressive strength by 18% and 27%, respectively, compared to the ground biochar (GB) batch. In contrast, higher dosages of NaOH (1% and 2%) resulted in 25% and 17% lower compressive strength, respectively, relative to the ground biochar (GB) batch. As the NaOH addition in biochar worked as an activator for the binder, it helped to accelerate the cement hydration kinetics in the initial stage[55] (Figure 6c). As a result, the 7 day compressive strength was comparatively higher in all of the Na-containing batches than the ground biochar batches. However, the reduction in strength after 28 days at higher NaOH dosages can be attributed to increased capillary porosity within the mortar matrix compared to the alkali-free system.[49] As observed from Figure 4, all of the biochar-containing batches showed reduced strength compared to the control batch. However, to assess whether such reductions were statistically significant, the *t*-test was performed. The test was performed with a 95% confidence level and provided the *p*-values for different batches. In this analysis, *p*-values greater than 0.05 indicate that the difference is not statistically significant, while *p*-values less than 0.05 indicate that the difference is statistically significant in compressive strength due to the use of biochar. Table S8 presents the *p*-values of different biochar batches at both 7 and 28 days of curing conditions compared to the control batch. It

https://doi.org/10.1021/acssusresmgt.5c00158
ACS Sustainable Resour. Manage. XXXX, XXX, XXX−XXX

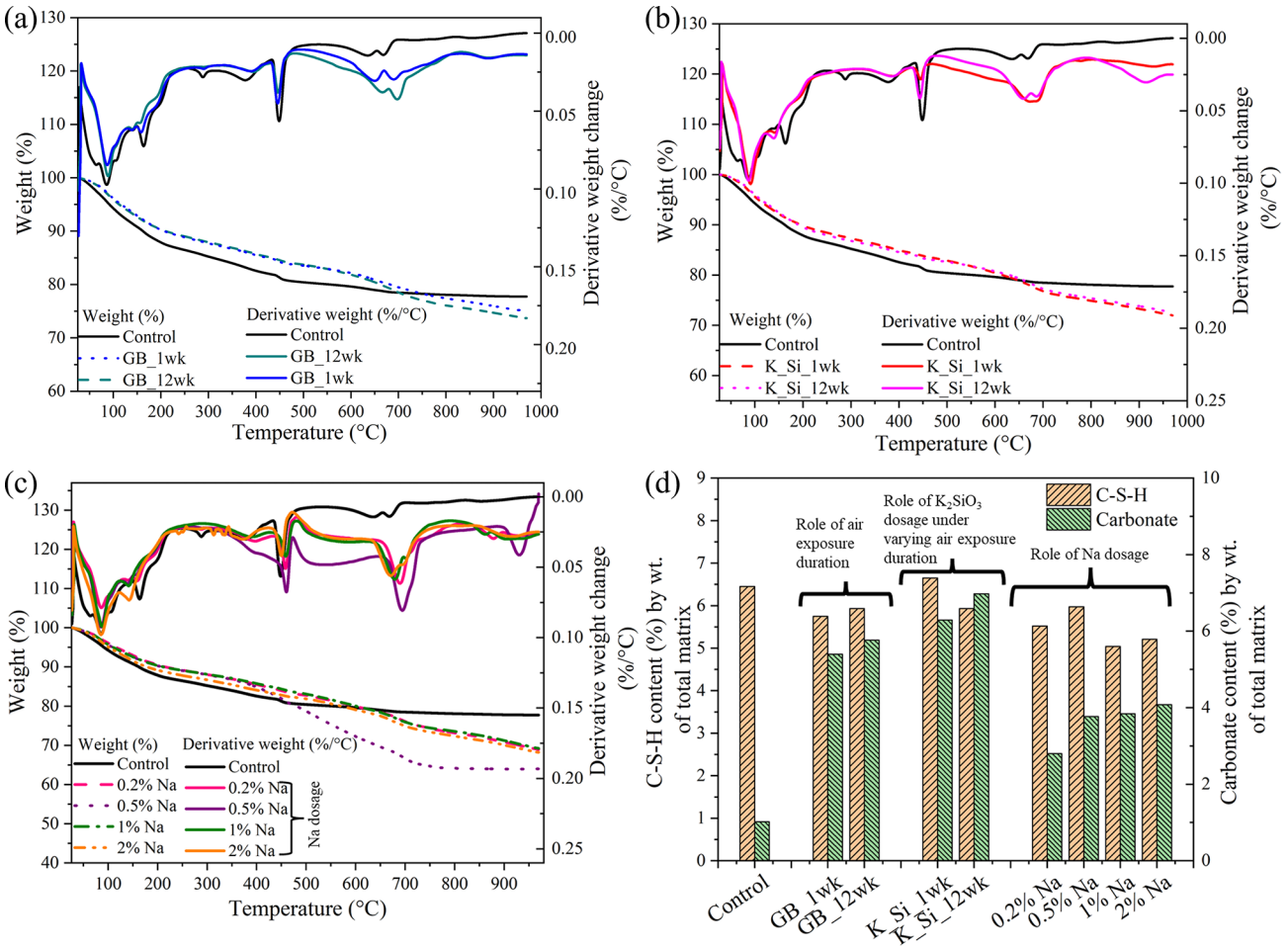

Figure 7. Thermogravimetric analysis of paste samples after 28 days of sealed curing of different biochar batches: (a) effect of biochar exposure to air for different durations, (b) effect of K_2SiO_3 dosage in biochar under varying air exposure durations, (c) effect of NaOH dosage in biochar, and (d) C−S−H and carbonate content of different biochar batches.

is observed that the *p*-values of the K_Si_1wk, 0.2% Na, and 0.5% Na batches were greater than 0.05, indicating that their compressive strengths were not statistically different (i.e., lower) from those of the control (without biochar). This corroborates that these three biochar-modified batches achieved mechanical performance comparable to that of the control, despite containing 30% biochar. However, all other batches exhibited *p*-values of less than 0.05, indicating that the compressive strength of these batches was drastically reduced compared to that of the control batch. As a result, it is also evident from the statistical analysis that the K_Si_1wk, 0.2% Na, and 0.5% Na batches exhibited significantly higher compressive strength compared to the other biochar batches.

As observed in Figure 4, the 7 day compressive strength of different NaOH- and K_2SiO_3-containing biochar batches was significantly higher than that of the GB_1wk and GB_12wk batches. As discussed previously, the addition of NaOH or K_2SiO_3 to biochar acted as an activator for the binder, helping to accelerate the cement hydration kinetics in the initial stage (Figure 6). As a result, the 7 day compressive strength was comparatively higher in all the NaOH- or K_2SiO_3-containing batches than the ground biochar batches. Table S9 represents the *p*-values of different NaOH- and K_2SiO_3-containing biochar batches at 7 day curing conditions, which are compared with the GB_12wk batch. It is evident from Table S9 that all of the biochar batches, except GB_1wk, exhibited *p*-values less than 0.05, indicating that the compressive strength of the NaOH- and K_2SiO_3-containing biochar batches significantly improved after 7 day curing conditions compared to the GB_12wk batch. The only exception was the GB_1wk batch (p = 0.23), which did not differ significantly from GB_12wk, highlighting that unmodified biochar does not provide significant early strength benefits only by extending the air exposure duration of biochar.

Effects of Biochar Modification on Cement Hydration Kinetics. Figure 6a represents the effect of biochar exposure to air for different durations on the hydration kinetics of the paste samples. The initial dissolution peak intensity for all of the biochar-containing batches is higher than that of the control batch. The heat flow peak for the GB_12wk batch shifted left compared to the GB_1wk and control batch, indicating a prominent cement hydration acceleration effect (Figure 6a). As discussed earlier, a longer duration of exposure to air allows for more CO_2 adsorption by the biochar (Figure 2a). The incorporation of CO_2 is known to accelerate the cement hydration reaction, leading to a faster heat release[56,57] and resulting in a quicker setting time (Figure 6a).

Figure 6b illustrates the effect of K−Si-modified biochar on hydration kinetics. The primary hydration peak of the K_Si_12wk batch, corresponding to the formation of hydration products, shifted significantly to the left. This indicates that prolonged exposure of the K_Si_12wk batch to

https://doi.org/10.1021/acssusresmgt.5c00158
ACS Sustainable Resour. Manage. XXXX, XXX, XXX−XXX

the air significantly accelerated the initial hydration process. This is also evident from Figure 6b, which shows that the heat release from the K_Si_12wk batch was higher initially than the K_Si_1wk batch. As a result, the dormant period for the K_Si_12wk batch was reduced significantly compared to the control and K_Si_1wk batch. Such an acceleration effect of the 12 week air-exposed sample was attributed to the additional carbonate phase present in this biochar sample (observed from TGA) in the form of K_2CO_3. This carbonate phase can dissolve in mixed water rapidly to form K^+ and HCO_3^- ions, both of which can accelerate the cement hydration.

Figure 6c illustrates the impact of varying the NaOH dosage in biochar on the hydration kinetics of the mortar samples. Figure 6c shows that the initial hydration peak moved to the left as the Na dosage increased. This shift indicates an acceleration effect resulting from the addition of NaOH in biochar. The presence of NaOH enhanced the dissolution of binder particles, increasing the availability of silica and alumina ions in the system.[58,59] At a lower NaOH dosage, the hydration process showed a moderate acceleration in the reaction rates. However, as the NaOH dosage increased, the dissolution of the binder components intensified, leading to faster hydration kinetics. This resulted in a shorter dormant period and increased the hydration reaction in the acceleration period for Na-containing batches compared to the control batch.[60,61]

To summarize, after 7 days, the total heat release of all of the biochar batches is higher than the control. Ground biochar provided an additional surface area to nucleate the hydration products due to its filler effect. This indicates that more cement underwent hydration in the biochar batches, resulting in more efficient cement utilization in comparison to the control.

Effects of Biochar Addition on the Microstructural Phase Assemblage. Figure 7 illustrates the TGA plots of different batches after 28 days of sealed curing. Calcium silicate hydrate (C−S−H) generally shows water loss from 50 °C to 600 °C, whereas carbonates decompose above 550 °C.[44,62] The biochar decomposition also starts from around 300 °C. Therefore, in this study, mass losses from 105 °C to 300 °C were considered to determine the C−S−H content, thereby avoiding the influence of evaporable water, biochar, portlandite, and carbonate phases. The range of 550−900 °C was used to measure the carbonate content in the paste samples. The 400 °C to 500 °C range was considered to calculate the portlandite content (CH),[62] and the weight loss between 105 °C and 600 °C was considered to calculate the chemically bound water in the paste samples.[21] However, biochar also decomposes in the same temperature range (Figure 2). Therefore, the calculation of C−S−H, carbonate, portlandite, and chemically bound water content in paste samples was revised to consider the weight loss from biochar decomposition, which was done according to a previously published work.[21] Figure 7d represents the C−S−H and carbonate contents, and Figure S1 represents the portlandite (CH) and chemically bound water contents in different batches after adjusting the biochar decomposition. Detailed calculations of carbonate, C−S−H, portlandite, and chemically bound water are provided in Tables S10−S13.

All biochar batches exhibited higher weight loss in the 550−900 °C range compared to the control batch, indicating higher carbonate formation (Figure 7d). This is attributed to the biochar's exposure to air for 1 or 12 weeks, during which it adsorbed atmospheric CO_2 that subsequently contributed to different carbonate formations during cement hydration. As per Figure 7a,b, the weight loss associated with carbonate decomposition of GB_12wk and K_Si_12wk batches was higher than that of 1 week batches, highlighting the porous biochar's enhanced capacity to sequester CO_2 over time and aiding in higher carbonate formation.[9] The carbonate content also gradually increased with a higher NaOH dosage in biochar. Notably, the batch with 2% Na exhibited a 46% higher carbonate content than that of the batch containing 0.2% Na, demonstrating the influence of Na treatment on carbonate formation.

Figure 7d shows that the control batch exhibited the highest mass loss up to 300 °C, indicating a greater presence of hydrated products such as C−S−H. In contrast, all biochar-incorporated batches exhibited lower mass loss in this temperature range, primarily due to the dilution effect caused by the partial replacement of cementitious materials with biochar. A similar trend was observed in the chemically bound water results (Figure S1). The lower bound water content of biochar-containing samples compared to the control, further confirms the dilution effect. However, among all the biochar batches, the K_Si_1wk batch had the highest chemically bound water and C−S−H content, which is consistent with the mechanical performance of this batch. Specifically, the K_Si_1wk batch demonstrated 8% and 18% higher C−S−H than the K_Si_12wk and 1% Na batches (the lowest strength batch), respectively, resulting in the highest strength among all the biochar batches. Notably, there is no significant variation in C−S−H content between the GB_1wk and GB_12wk batches. Moreover, it was observed from the FTIR analysis (Figure S2) that the inclusion of various modified biochars did not alter the polymerization of the C−S−H gel.

Effects of Engineered Biochar on the Environmental Impact. As shown in Figure 8, the control mortar batch that did not contain biochar had a very high carbon footprint of 277.4 kg of CO_2 eq/m^3 of mortar. All mortar batches had a biochar dosage of 30% of the binder mass and followed the same production method with and without additives. Consequently, the carbon footprint changes in biochar batches mainly relied on their physical carbon storage capacity and the CO_2 sequestration ability of the binder matrix when combined with various biochar samples. To calculate the overall GWP value of mortar samples (Figure 8), total emission from each of the materials, including biochar, was calculated and then

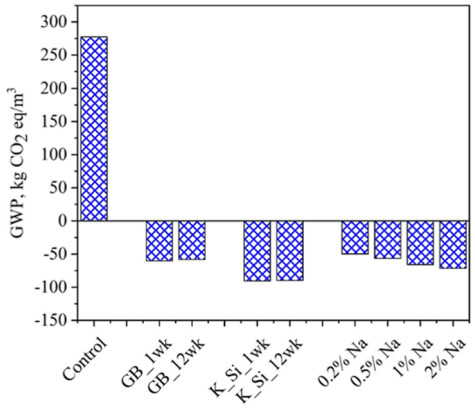

Figure 8. Global warming potential (GWP) of different biochar-containing mortar batches.

https://doi.org/10.1021/acssusresmgt.5c00158
ACS Sustainable Resour. Manage. XXXX, XXX, XXX−XXX

summed, which provided negative GWP values for biochar batches due to their high carbon sequestration capacity.

GB_1wk and GB_12wk biochar had comparable physical carbon content, ranging from 77% to 78%. Additionally, the CO_2 sequestration related to carbonate formation in the binder captured 19−20 kg of CO_2 per m^3 of mortar. Overall, these batches produced carbon-negative mortar with a GWP ranging from −58 to −60 kg CO_2 eq/m^3 of mortar.

Among all the batches, the biochar samples modified with K_2SiO_3 exhibited the highest carbon content, ranging from 86.4% to 87.2%. K, Si addition to biochar also facilitated increasing the binder CO_2 sequestration capacity, ranging from 22 to 24 kg/m^3. Overall, these mortar batches achieved the maximum negative carbon footprint, approximately −89.67 to −90.68 kg of CO_2 eq/m^3.

In Na-containing biochar batches, as the NaOH dosage increased from 0.2 to 2 wt % of the biochar feedstock, the physical carbon content of the biochar rose from 79% to 86%. The binder CO_2 sequestration was higher than the control batch, ranging from 9−14 kg CO_2/m^3. These batches also created carbon-negative mixtures, with a GWP varying between −49.80 and −71.53 kg CO_2 eq/m^3.

CONCLUSION

This paper presents an investigation on how altering the biochar properties can enhance its role as concrete additives. Overall, the effect of the 30% surface-modified biochar addition on the microstructural and mechanical properties of the mortar composites was investigated in this study.

The following conclusions can be drawn from this study:

I A longer exposure of biochar to air before using it in concrete is beneficial. This is because a longer exposure enables more CO_2 binding in the pores of biochar, which eventually enhances the performance of cementitious composites. Specifically, biochar exposed to air for 12 weeks improved the composite's 28 day compressive strength by 15% compared to biochar exposed for just 1 week.

II The K−Si-containing batch (exposed to air for 1 week) provided 44% higher 28 day compressive strength than the one containing pure biochar. The benefit of adding K_2SiO_3 before pyrolysis is attributed to the pozzolanic properties of the Si. However, such benefit of incorporating K−Si during biochar production was diminished for longer air exposure duration. Specifically, the K_Si_12wk and GB_12wk batches exhibited similar compressive strength. The diminished benefit of K−Si due to the air exposure was attributed to the agglomeration of SiO_2, as observed from the SEM image.

III The workability of biochar-containing mortar batches improved with increasing Na content in biochar. 0.5% Na batch (29 MPa) provided the maximum strength among other Na-containing batches after 28 days. This was 27% and 11% higher than the GB_1wk and GB_12wk batches, respectively. Na acted as a slag cement activator, enhancing the dissolution of raw materials during early hydration. However, higher Na addition (1% and 2%) in biochar reduced the strength significantly after 28 days due to the increased porosity in the mortar matrix caused by excessive Na. Therefore, the addition of Na, upto a certain dosage, during the production of biochar also improved its performance as concrete additives.

IV The cement hydration was enhanced by incorporating ground biochar, which offered additional surface area for the nucleation of cement hydration products. However, the initial hydration peak of batches containing 12 weeks air exposed biochar showed more prominent acceleration effect compared to the 1 week batches. This is attributed to the higher CO_2 adsorption of the 12 week batches, leading to a faster heat release during the initial stages of hydration.

V All the biochar batches resulted in a negative carbon footprint, with the K_Si_1wk and K_Si_12wk batches showing the maximum negative GWP of −90.68 kg CO_2 equivalent per m^3. The reduction in GWP of the biochar-containing mortar mixes compared to the control batch ranged from 117%−133%.

This research demonstrated the use of a higher dosage of biochar by modifying its surface properties to develop carbon-negative cementitious composites. Further investigation is needed as this study focuses on a single feedstock and does not address long-term durability under varying environmental conditions. Additionally, the large-scale applicability and long-term performance should be evaluated by using various feedstocks and surface modification strategies. However, this study successfully demonstrates the potential of using high-dosage surface-modified biochar for producing carbon-negative cementitious composites, achieving significant CO_2 sequestration and improved mechanical properties. It provides a novel framework for utilizing biochar as a multifunctional additive, paving the way for sustainable construction materials.

ASSOCIATED CONTENT

Supporting Information

The Supporting Information is available free of charge at https://pubs.acs.org/doi/10.1021/acssusresmgt.5c00158.

Casting procedure of mortar and paste samples; oxide content of OPC and slag cement; proximate and elemental analysis of pine particles; d_{50} values of different biochar batches after grinding for 1 h; mix design (kg/m^3); $Ca(OH)_2$ and chemically bound water content in the paste samples of different batches; FTIR spectra of 28 days sealed cured paste samples of different biochar batches: effect of biochar exposure to air for different durations, effect of K and Si dosage in biochar under varying air exposure durations, and effect of Na dosage in biochar; GWP data inventory; GWP values of different materials based on the Ecoinvent 3 database; GWP values of different biochar batches; total mortar GWP (kg CO_2 eq/m^3 of mortar) calculated using eq 3; statistical (*t*-test) analysis results (*p*-values) of compressive strength compared with respect to the control batch; statistical (*t*-test) analysis results (*p*-values) of compressive strength compared with respect to the GB_12wk batch; $CaCO_3$ calculation (without biochar adjustments and with biochar adjustments); C−S−H calculation (without biochar adjustments and with biochar adjustments); $Ca(OH)_2$ calculation (without biochar adjustments and with biochar adjustments); and chemically bound water calculation (without biochar adjustments and with biochar adjustments) (PDF)

https://doi.org/10.1021/acssusresmgt.5c00158
ACS Sustainable Resour. Manage. XXXX, XXX, XXX−XXX

AUTHOR INFORMATION

Corresponding Author

Warda Ashraf − *Department of Civil Engineering, University of Texas at Arlington, Arlington, Texas 76010, United States;* orcid.org/0000-0002-5867-5129; Email: warda.ashraf@uta.edu

Authors

Nishad Ahmed − *Department of Civil Engineering, University of Texas at Arlington, Arlington, Texas 76010, United States;* orcid.org/0009-0002-8499-8914

Adhora Tahsin − *Department of Civil Engineering, University of Texas at Arlington, Arlington, Texas 76010, United States;* orcid.org/0009-0001-6230-8911

Qiangu Yan − *1 Gifford Pinchot Drive, USDA Forest Service, Forest Products Laboratory, Madison, Wisconsin 53726-2398, United States*

Zhiyong Cai − *1 Gifford Pinchot Drive, USDA Forest Service, Forest Products Laboratory, Madison, Wisconsin 53726-2398, United States*

Complete contact information is available at: https://pubs.acs.org/10.1021/acssusresmgt.5c00158

Notes

The authors declare no competing financial interest.

ACKNOWLEDGMENTS

Funding for this research was provided by the US National Science Foundation (NSF EFRI-2318123 and PFI-TT-2329856). All opinions, findings, and conclusions or recommendations expressed in this material are those of the authors and do not necessarily reflect the views of the funding agencies.

REFERENCES

(1) Danish, A.; Salim, M. U.; Ahmed, T. Trends and developments in green cement A sustainable approach. *Sustain. Struct. Mater.* **2019**, *2* (1), 45−60.

(2) Makul, N.; et al. Capacity to develop recycled aggregate concrete in south east asia. *Buildings* **2021**, *11*, 234.

(3) Worrell, E.; Price, L.; Martin, N.; Hendriks, C.; Meida, L. O. Carbon dioxide emissions from the global cement industry 1. *Annu. Rev. Energy* **2001**, *26* (1), 303−329.

(4) Juenger, M. C. G.; Winnefeld, F.; Provis, J. L.; Ideker, J. H. Advances in alternative cementitious binders. *Cem. Concr. Res* **2011**, *41*, 1232.

(5) Ige, O. E.; Olanrewaju, O. A.; Duffy, K. J.; Collins, O. C. Environmental Impact Analysis of Portland Cement (CEM1) Using the Midpoint Method. *Energies* **2022**, *15* (7), 2708.

(6) Mehta, M. P. Greening of the Concrete Industry for Sustainable Development. *Concr. Int.* **2002**, *24* (7), 23−28.

(7) Mukherjee, A.; Zimmerman, A. R. Organic carbon and nutrient release from a range of laboratory-produced biochars and biochar−soil mixtures. *Geoderma* **2013**, *193*−*194*, 122−130.

(8) Bruun, E. W.; Ambus, P.; Egsgaard, H.; Hauggaard-Nielsen, H. Effects of slow and fast pyrolysis biochar on soil C and N turnover dynamics. *Soil Biol. Biochem.* **2012**, *46*, 73−79.

(9) Gupta, S.; Kua, H. W.; Low, C. Y. Use of biochar as carbon sequestering additive in cement mortar. *Cem. Concr. Compos.* **2018**, *87*, 110−129.

(10) Břendová, K.; Tlustoš, P.; Száková, J.; Száková, J.; Habart, J. Biochar properties from different materials of plant origin. *Eur. Chem. Bull.* **2012**, *1*, 535−539.

(11) Gupta, S.; Kua, H. W.; Koh, H. J. Application of biochar from food and wood waste as green admixture for cement mortar. *Sci. Total Environ.* **2018**, *619*−*620*, 419−435.

(12) McBeath, A. V.; Wurster, C. M.; Bird, M. I. Influence of feedstock properties and pyrolysis conditions on biochar carbon stability as determined by hydrogen pyrolysis. *Biomass Bioenergy* **2015**, *73*, 155−173.

(13) Lehmann, J.; Gaunt, J.; Rondon, M. Bio-char Sequestration in Terrestrial Ecosystems—A Review. *Mitig Adapt Strateg Glob Chang* **2006**, *11* (2), 403−427.

(14) Leturcq, P. GHG displacement factors of harvested wood products: the myth of substitution. *Sci. Rep.* **2020**, *10* (1), 20752.

(15) Roberts, K. G.; Gloy, B. A.; Joseph, S.; Scott, N. R.; Lehmann, J. Life Cycle Assessment of Biochar Systems: Estimating the Energetic, Economic, and Climate Change Potential. *Environ. Sci. Technol.* **2010**, *44* (2), 827−833.

(16) Suarez-Riera, D.; Restuccia, L.; Ferro, G. A. The use of Biochar to reduce the carbon footprint of cement-based materials. *Procedia Struct. Integr.* **2020**, *26*, 199−210.

(17) Restuccia, L.; Ferro, G. A. Promising low cost carbon-based materials to improve strength and toughness in cement composites. *Constr. Build. Mater.* **2016**, *126*, 1034−1043.

(18) Ahmad, S.; Khushnood, R. A.; Jagdale, P.; Tulliani, J.-M.; Ferro, G. A. High performance self-consolidating cementitious composites by using micro carbonized bamboo particles. *Mater. Des.* **2015**, *76*, 223−229.

(19) Li, Z.; Shi, X. Towards sustainable industrial application of carbon-negative concrete: Synergistic carbon-capture by concrete washout water and biochar. *Mater. Lett.* **2023**, *342*, 134368.

(20) Chen, L.; et al. Biochar-augmented carbon-negative concrete. *Chem. Eng. J.* **2022**, *431*, 133946.

(21) Ahmed, N.; Tahsin, A.; Nishat, F. M.; Ashraf, W. Functionalized biochar for carbon neutral/negative cementitious composites with superior performances. *Constr. Build. Mater.* **2025**, *458*, 139143.

(22) Tan, K.; Pang, X.; Qin, Y.; Wang, J. Properties of cement mortar containing pulverized biochar pyrolyzed at different temperatures. *Constr. Build. Mater.* **2020**, *263*, 120616.

(23) Chen, T.; Zhao, L.; Gao, X.; Li, L.; Qin, L. Modification of carbonation-cured cement mortar using biochar and its environmental evaluation. *Cem. Concr. Compos.* **2022**, *134*, 104764.

(24) Gupta, S.; Kua, H. W.; Tan Cynthia, S. Y. Use of biochar-coated polypropylene fibers for carbon sequestration and physical improvement of mortar,". *Cem. Concr. Compos.* **2017**, *83*, 171−187.

(25) Hagemann, N.; Spokas, K.; Schmidt, H.-P.; Kägi, R.; Böhler, M.; Bucheli, T. Activated Carbon, Biochar and Charcoal: Linkages and Synergies across Pyrogenic Carbon's ABCs. *Water* **2018**, *10* (2), 182.

(26) Arabzadeh Nosratabad, N.; Yan, Q.; Cai, Z.; Wan, C. "Exploring nanomaterial-modified biochar for environmental remediation applications,". *Heliyon* **2024**, *10* (18), No. e37123.

(27) Murtaza, G.; et al. "Recent trends and economic significance of modified/functionalized biochars for remediation of environmental pollutants,". *Sci. Rep.* **2024**, *14* (1), 217.

(28) Ramola, S.; Mohan, D.; Masek, O.; Méndez, A.; Tsubota, T. *Engineered Biochar Fundamentals, Preparation, Characterization and Applications*; Springer Nature, 2022; .

(29) Chen, W.; et al. A new insight into chemical reactions between biomass and alkaline additives during pyrolysis process. *Proc. Combust. Inst.* **2021**, *38* (3), 3881−3890.

(30) Li, K.; et al. Influence of aged biochar modified by Cd2+ on soil properties and microbial community. *Sustainability* **2020**, *12* (12), 4868.

(31) Cui, Z.; Wang, Y.; Wang, N.; Ma, F.; Yuan, Y. Effects of Ageing on Surface Properties of Biochar and Bioavailability of Heavy Metals in Soil. *Agriculture* **2024**, *14* (9), 1631.

(32) Yan, Q.; Nosratabad, N. A.; Du, X.; Ketelboeter, T.; Wan, C.; Cai, Z. Highly effective lead removal by novel alkaline biochar prepared by pyrolysis of woody biomass impregnated with low-level NaOH. *J. Hazard. Mater. Adv.* **2025**, *18*, 100657.

(33) Wang, H.; Feng, M.; Zhou, F.; Huang, X.; Tsang, D. C. W.; Zhang, W. Effects of atmospheric ageing under different temperatures on surface properties of sludge-derived biochar and metal/metalloid stabilization. *Chemosphere* **2017**, *184*, 176−184.
(34) Yang, X.; et al. Surface functional groups of carbon-based adsorbents and their roles in the removal of heavy metals from aqueous solutions. *Chem. Eng. J.* **2019**, *366* (366), 608−621.
(35) Chen, X.; Lewis, S.; Heal, K. V.; Lin, Q.; Sohi, S. P. Biochar engineering and ageing influence the spatiotemporal dynamics of soil pH in the charosphere. *Geoderma* **2021**, *386* (386), 114919.
(36) Guo, D.; Wu, S.; Liu, B.; Yin, X.; Yang, Q. Catalytic effects of NaOH and Na2CO3 additives on alkali lignin pyrolysis and gasification. *Appl. Energy* **2012**, *95*, 22.
(37) Wongmat, Y.; Wagner, D. R. Effect of Potassium Salts on Biochar Pyrolysis. *Energies* **2022**, *15* (16), 5779.
(38) Advanced Standards Transforming Markets C1437 Standard Test Method for Flow of Hydraulic Cement Mortar 2007. www.astm.org (accessed Oct 14, 2020).
(39) Advanced Standards Transforming Markets C109,Standard Test Method for Compressive Strength of Hydraulic Cement Mortars (Using 2-in. or [50-mm] Cube Specimens) 2009. www.astm.org (accessed Mar 12, 2020).
(40) Xia, F.; Zhang, Z.; Zhang, Q.; Huang, H.; Zhao, X. Life cycle assessment of greenhouse gas emissions for various feedstocks-based biochars as soil amendment. *Sci. Total Environ.* **2024**, *911*, 168734.
(41) Puettmann, M.; Sahoo, K.; Wilson, K.; Oneil, E. Life cycle assessment of biochar produced from forest residues using portable systems. *J. Cleaner Prod.* **2020**, *250*, 119564.
(42) Sahoo, K.; Upadhyay, A.; Runge, T.; Bergman, R.; Puettmann, M.; Bilek, E. Life-cycle assessment and techno-economic analysis of biochar produced from forest residues using portable systems. *Int. J. Life Cycle Assess.* **2020**, *26*, 189−213.
(43) Azzi, E. S.; Karltun, E.; Sundberg, C. Prospective Life Cycle Assessment of Large-Scale Biochar Production and Use for Negative Emissions in Stockholm. *Environ. Sci. Technol.* **2019**, *53* (14), 8466−8476.
(44) Wei, H.; et al. Granular Bamboo-Derived Activated Carbon for High CO2 Adsorption: The Dominant Role of Narrow Micropores. *ChemSusChem* **2012**, *5* (12), 2354−2360.
(45) Shafeeyan, M. S.; Daud, W. M. A. W.; Houshmand, A.; Arami-Niya, A. Ammonia modification of activated carbon to enhance carbon dioxide adsorption: Effect of pre-oxidation. *Appl. Surf. Sci.* **2011**, *257* (9), 3936−3942.
(46) Ghani, W. A. W. A. K.; et al. Biochar production from waste rubber-wood-sawdust and its potential use in C sequestration: Chemical and physical characterization. *Ind. Crops Prod.* **2013**, *44*, 18−24.
(47) Cui, X.; Li, M.; Chen, X.; Shao, Y.; Li, Y.; Zuo, J.; Li, J. Effect of addition of K2CO3 on the structure of coals with different ranks by FTIR and TG/MS. *J. Anal. Appl. Pyrolysis* **2023**, *172*, 106027.
(48) Sergeev, D.; Yazhenskikh, E.; Kobertz, D.; Müller, M. Vaporization behavior of Na2CO3 and K2CO3. *Calphad* **2019**, *65*, 42−49.
(49) Keiluweit, M.; Nico, P. S.; Johnson, M. G.; Kleber, M. Dynamic Molecular Structure of Plant Biomass-Derived Black Carbon (Biochar). *Environ. Sci. Technol.* **2010**, *44* (4), 1247−1253.
(50) Siipola, V.; et al. Effects of biomass type, carbonization process, and activation method on the properties of bio-based activated carbons. *Bioresources* **2018**, *13* (3), 5976−6002.
(51) Yang, P.; Yang, H.; Wang, N.; Du, C.; Pang, S.; Zhang, Y. Hygroscopicity measurement of sodium carbonate, *β*-alanine and internally mixed *β*-alanine/Na2CO3 particles by ATR-FTIR. *J. Environ. Sci.* **2020**, *87*, 250−259.
(52) Tahsin, A.; Borno, I. B.; Ahmed, N.; Nair, N.; Ashraf, W.; Hollenbeck, C. Evaluation of low-carbon cementitious composites in marine environment for coastal protection and artificial reef substrate. *npj Mater. Degrad.* **2025**, *9* (1), 116.
(53) Wu, H.-C.; Sun, P. Effect of Mixture Compositions on Workability and Strength of Fly Ash-Based Inorganic Polymer Mortar. *ACI Mater. J.* **2010**, *107* (6), 554−562.
(54) Zhang, D.; Zhao, J.; Wang, D.; Wang, Y.; Ma, X. Influence of pozzolanic materials on the properties of natural hydraulic lime based mortars. *Constr. Build. Mater.* **2020**, *244*, 118360.
(55) Zhang, M.; Zunino, F.; Yang, L.; Wang, F.; Scrivener, K. Understanding the negative effects of alkalis on long-term strength of Portland cement. *Cem. Concr. Res.* **2023**, *174*, 107348.
(56) Monkman, S.; MacDonald, M.; Hooton, R. D.; Sandberg, P. Properties and durability of concrete produced using CO2 as an accelerating admixture. *Cem. Concr. Compos.* **2016**, *74*, 218−224.
(57) Monkman, S.; Lee, B. E. J.; Grandfield, K.; MacDonald, M.; Raki, L. The impacts of in-situ carbonate seeding on the early hydration of tricalcium silicate. *Cem. Concr. Res.* **2020**, *136*, 106179.
(58) Jawed, I.; Skalny, J. Alkalies in cement: A review: II. Effects of alkalies on hydration and performance of Portland cement. *Cem. Concr. Res.* **1978**, *8* (1), 37−51.
(59) Rattanasak, U.; Chindaprasirt, P. Influence of NaOH solution on the synthesis of fly ash geopolymer. *Miner. Eng.* **2009**, *22* (12), 1073−1078.
(60) Mota, B.; Matschei, T.; Scrivener, K. Impact of NaOH and Na2SO4 on the kinetics and microstructural development of white cement hydration. *Cem. Concr. Res.* **2018**, *108*, 172−185.
(61) Zheng, Z.; et al. Insights into the effect of NaOH on the hydration products of solidified cement-NaNO3 matrices and leaching behavior of Sr2+. *Sci. Total Environ.* **2021**, *755*, 142581.
(62) Scrivener, K.; Snellings, R.; Lothenbach, B. *A practical guide to microstructural analysis of cementitious materials*; CRC Press, 2016; .

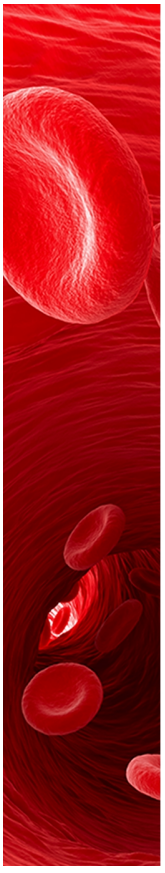
CAS BIOFINDER DISCOVERY PLATFORM™
CAS BIOFINDER HELPS YOU FIND YOUR NEXT BREAKTHROUGH FASTER
Navigate pathways, targets, and diseases with precision
Explore CAS BioFinder
CAS
A division of the American Chemical Society

https://doi.org/10.1021/acssusresmgt.5c00158
ACS Sustainable Resour. Manage. XXXX, XXX, XXX−XXX